

RESEARCH ARTICLE

Biomechanical properties of 3D printable material usable for synthetic personalized healthy human aorta

SiYu Lin^{1*}, Georges Tarris², Chloe Bernard³, Moundji Kafi³, Paul M. Walker^{1,4}, Diana M. Marín-Castrillón¹, Camille Gobled⁵, Arnaud Boucher¹, Benoit Presles¹, Marie Catherine Morgant^{1,3}, Alain Lalande^{1,4}, Olivier Bouchot^{1,3}

¹ImViA Laboratory, EA 7535, University of Burgundy, Dijon, France

²Department of Pathology, University Hospital of Dijon, Dijon, France

³Department of Cardio-Vascular and Thoracic Surgery, University Hospital of Dijon, Dijon, France

⁴Department of Medical Imaging, University Hospital of Dijon, Dijon, France

⁵ENNOIA Company, Besançon, France

Abstract

With the development of three-dimensional (3D) printing, 3D-printed products have been widely used in medical fields, such as plastic surgery, orthopedics, dentistry, etc. In cardiovascular research, 3D-printed models are becoming more realistic in shape. However, from a biomechanical point of view, only a few studies have explored printable materials that can represent the properties of the human aorta. This study focuses on 3D-printed materials that might simulate the stiffness of human aortic tissue. First, the biomechanical properties of a healthy human aorta were defined and used as reference. The main objective of this study was to identify 3D printable materials that possess similar properties to the human aorta. Three synthetic materials, NinjaFlex (Fenner Inc., Manheim, USA), Filastic™ (Filastic Inc., Jardim Paulistano, Brazil), and RGD450+TangoPlus (Stratasys Ltd.®, Rehovot, Israel), were printed in different thicknesses. Uniaxial and biaxial tensile tests were performed to compute several biomechanical properties, such as thickness, stress, strain, and stiffness. We found that with the mixed material RGD450+TangoPlus, it was possible to achieve a similar stiffness to healthy human aorta. Moreover, the 50-shore-hardness RGD450+TangoPlus had similar thickness and stiffness to the human aorta.

Keywords: 3D printing; Biomechanical property; Human aorta; Tensile test

*Corresponding author:

SiYu Lin (siyu.lin@u-bourgogne.fr)

Citation: Lin S, Tarris G, Bernard C, et al., 2023, Biomechanical properties of 3D printable material usable for synthetic personalized healthy human aorta. *Int J Bioprint*. <https://doi.org/10.18063/ijb.736>

Received: September 09, 2022

Accepted: January 27, 2023

Published Online: April 20, 2023

Copyright: © 2023 Author(s).

This is an Open Access article distributed under the terms of the Creative Commons Attribution License, permitting distribution and reproduction in any medium, provided the original work is properly cited.

Publisher's Note: Whioce Publishing remains neutral with regard to jurisdictional claims in published maps and institutional affiliations.

1. Introduction

Three-dimensional (3D) printing has been widely used in various fields. The technology uses computational 3D imaging software to sort out tomographic data in order to produce 3D reconstruction images. This information can be regenerated into standard tessellation language (STL) files. In recent years, medical fields such as plastic surgery, orthopedics, dentistry, etc. have also begun to apply 3D printing^[1-6]. The main

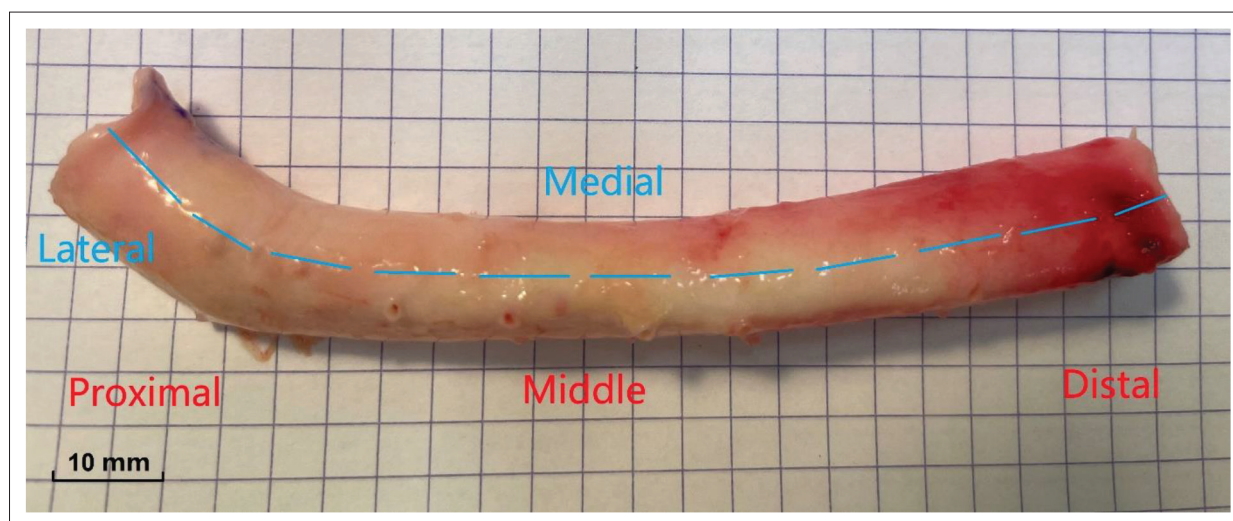


Figure 1. Healthy aortic sample taken during the autopsy of a 16-year-old boy who died from pulmonary embolism. The orientation of the aorta (medial and lateral in blue; proximal, middle, and distal in red) is indicated on the image. Perforating medullary arteries are also seen in the image.

procedures in iatrical use can be summarized into two steps: modeling personalized geometry from computerized tomography (CT) or magnetic resonance (MR) images, and then printing as a prosthesis. Existing applications in the cardiovascular field mainly focus on education and preoperative simulation^[7-10]. The aim of these studies has been to simulate the shape of human aortas, arteries, or valves, rather than their biomechanical properties; thus, the majority of printed aortas and arteries are made with hard material. There are more than two reasons to explain the need for the development of an aortic representable syntactic material. First, due to variations in tensile test machine measurements, the result from one study is not always comparable to another^[11]. Considering that the aortic wall exhibits biomechanical characteristics such as nonlinearity, anisotropy, and low stiffness^[11,12], proposing a common syntactic material could be helpful to elaborate aortic biomechanical experiments^[13]. Experiments that have been performed with the synthetic material should be reproducible and as close as possible to the real aorta. Second, computational fluid dynamic (CFD) and fluid-structure interaction (FSI) analyses have been widely applied in the simulation of aortic dilatation or other aortic diseases^[14-16]. However, a common limitation of these studies is the lack of validation, especially for studies based on phantoms^[17-19]. Building a phantom with an aortic representable synthetic material would appear to be essential if experiments are to be extended to living aortic tissue. A baseline for aortic simulation might be possible through an image analysis of the phantom^[20]. Such a study does not require biocompatible materials. As far as we know, very few studies have explored the use of soft materials in printing arteries^[21-24]. A common soft material used in

these studies is the rubber-like material TangoFLX930TM (Stratasys Ltd.®, Israel). These studies have dealt with the pulmonary artery, mitral valve, and cerebral vessels. The reported stiffness value in these studies is lower than that of the human aorta^[11]. The aim of our present study was to identify printable materials that could better represent the human aorta.

2. Materials and method

2.1. Materials

A fresh healthy human aorta was obtained from an autopsy from the Department of Pathology, University Hospital of Dijon, Dijon, France (Figure 1). The patient was 16 years old and died from pulmonary embolism at the hospital. The patient had no underlying health conditions. With regard to Jardé law (French Bioethics law), patient consent was waived as autopsy samples are not concerned by bioethical regulations. The sample (11 cm in length) corresponded to the descending thoracic aortic wall (beginning after the left subclavian artery, extending down, and terminating at the start of the abdominal aorta), with perforating medullary arteries seen as small holes in Figure 1.

The aortic sample was visually separated into the medial aortic quadrant (smaller curvature of the aortic wall), lateral aortic quadrant (greater curvature of the aortic wall), proximal aorta, middle aorta, and distal aorta. Six specimens were obtained: one in the medial proximal area, two in the medial middle area, one in the lateral middle area, one in the medial distal area, and one in the lateral distal area.

Several thermoplastic polyurethane and rubber-like materials were tested as 3D-printable materials that could

mimic the biomechanical properties of a human aorta. These synthetic materials are not biocompatible. Therefore, phantoms were used to carry out the biomechanical study and simulation. Two groups of materials were tested: thermoplastic polyurethane and rubber-like materials.

2.1.1. Thermoplastic polyurethane

Two thermoplastic polyurethane materials, NinjaFlex (Fenner Inc., Mannheim, USA) and Filastic™ (Filastic Inc., Jardim Paulistano, Brazil) were provided by Dijon 3D Company (Dijon, France). The NinjaFlex material was printed at a temperature of 225°C–235°C. Heating plates were not required during printing. The printing speed was 15–35 milliseconds per meter. The MakerBot (MakerBot Industries, USA) 3D printer equipped with a Thingiverse driver block (MakerBot Industries, USA) was dedicated to NinjaFlex printing. The machine was kept at a strict horizontal position during the printing process. In order to minimize printing errors (within 0.05 mm), the 3D printing machine was adjusted by a standard scale. The diameter of the original material was 1.75 mm, with 85 shore hardness (SH). For experimental purposes, different thicknesses of NinjaFlex material were printed, ranging from 0.2 mm to 1.8 mm in 15 mm × 15 mm squares. Due to printing process issues and low thickness managements, samples ranging in thickness from 0.2 mm to 0.7 mm were excluded in this study. Phantoms from the second material, the 85-SH Filastic™, were printed at a nozzle temperature of 220°C–240°C. A heating plate was necessary for printing, and the heating stability should be 100°C–110°C. During the printing process, the distance between the gear and the printing tube was controlled to be constantly less than 5 mm. The thickness interval of the material could only be controlled within 0.05 mm due to the material's characteristics. Different thicknesses of Filastic™ were printed, ranging from 0.5 mm to 0.85 mm in 40 mm × 40 mm squares.

2.1.2. Rubber-like material (RGD450+TangoPlus)

RGD450+TangoPlus is an advanced rubber-like material that can be printed with a smooth surface by ENNOIA Company (Besançon, France) using the Connex3™ Object500 3D printer (Stratasys Ltd., Israel). It is a composite material of RGD450 and TangoPlus (Stratasys Ltd., Israel). Materials of different shore hardness were printed and tested (Table 1). Although the size of the printed RGD450+TangoPlus specimens was 40 mm × 40 mm, the size of the tested RGD450+TangoPlus specimens was only 15 mm × 15 mm. Figure 2 shows the printed RGD450+TangoPlus specimens. The tested specimens maintained directional consistency during testing. The direction was fixed according to the biaxial test system and was defined as A and B.

Table 1. RGD450+TangoPlus material printed with different shore hardness and thicknesses

Thickness of RGD450+TangoPlus material (mm)				
70 SH	2			
60 SH	2			
50 SH	2	2.5	3	3.5
40 SH	2.5	3	3.5	4

2.2. Method

The aortic wall sample from a healthy patient was preserved in phosphate-buffered saline during the transfer from the autopsy room to the laboratory for tensile experiment. Due to the regional differences in biomechanical properties of the aortic wall^[12], the samples were cut into smaller square samples (15 mm × 15 mm) in order to mimic standard equibiaxial experiments on aortic tissue. The average thickness was measured using an electronic micrometer (Litematic VL-50, Mitutoyo®, Japan) before loading. Each aortic specimen was labeled according to their circumferential and longitudinal directions with respect to the blood flow in the aorta. Biomechanical experiments were carried out using a biaxial tensile test machine (LM1 Planar Biaxial, TA Instruments, USA, Figure 3). The preconditioning was set to 10% of the experimental sample length (10 mm), with 10 loading-unloading repetitions.

Only uniaxial tests were performed on the thermoplastic polyurethane material due to its isotropic behavior during the printing process, whereas biaxial tensile tests were performed on the healthy human aorta and the rubber-like material. All tensile tests were repeatedly performed, and surgical hooks were used to secure the connection between the sample and the system. Only one result per material per thickness was preserved in our study: the one with the smoothest stress–strain curve.

The maximum Young's modulus, also known as the elastic modulus, was calculated for the evaluation of sample stiffness^[25]. The printed material was studied according to three parameters: thickness, the maximum value of Young's modulus, and the stress–strain curves.

3. Result

3.1. Thickness and maximum Young's modulus

There was a difference between the expected printed thickness and the experimentally measured thickness (Tables 3 and 4). Nevertheless, the maximum Young's modulus was compared among materials.

3.1.1. Human aorta

The aortic wall had a mean thickness of 1.49 ± 0.34 mm. The mean failure stress and maximum Young's modulus

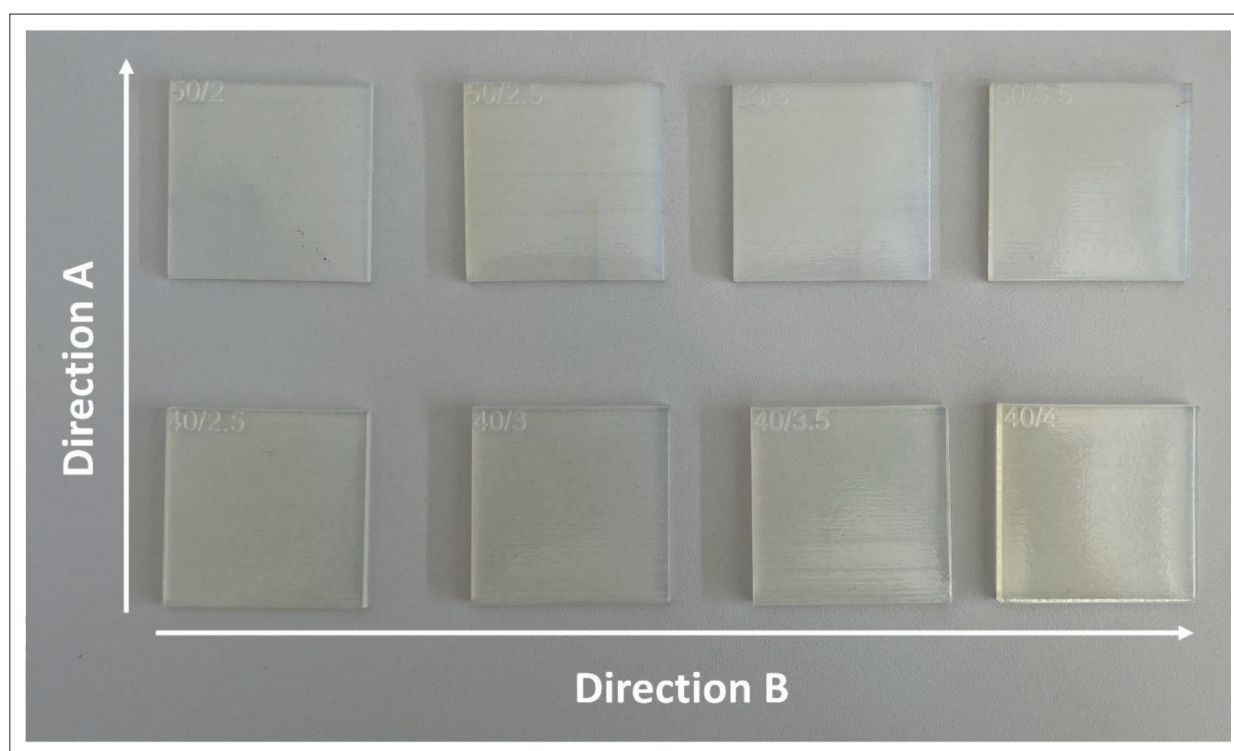


Figure 2. Printed RGD450+TangoPlus samples (40 mm × 40 mm) of 40 SH and 50 SH (from left to right: 2.5 mm, 3 mm, 3.5 mm, and 4 mm in thickness).

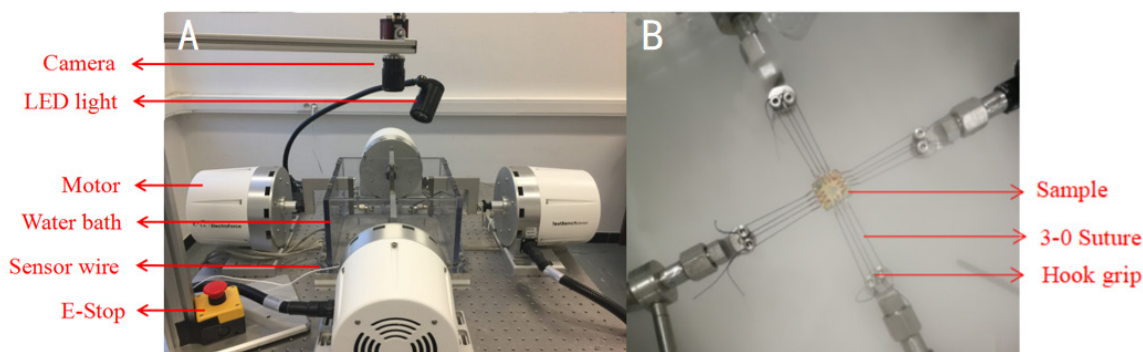


Figure 3. Biaxial tensile test machine and sample placement. (A) Biaxial tensile test machine (LM1 Planar Biaxial, TA Instruments, USA). (B) Sample placement during the test. Abbreviation: LED, light-emitting diode.

were 0.48 ± 0.09 MPa and 0.91 ± 0.23 MPa, respectively (Table 2).

3.1.2. Thermoplastic polyurethane

The thickness, failure stress, and maximum Young's modulus of the tested NinjaFlex material are shown in Table 3. There was a noticeable discrepancy between the thickness measured in the experiments and the thickness set at printing. The maximum difference was observed in the NinjaFlex specimen with a nominal 1.7 mm thickness (10.12%). On the other hand, the NinjaFlex specimen with a 0.9 mm thickness had the smallest difference (1.67%).

As the thickness of the NinjaFlex material increases, its failure stress showed a general increasing trend; however, its stiffness did not show a steadily increasing trend. The maximum Young's modulus ranged from 8.24 to 11.90 MPa.

Upon testing the Filastic™ material with different thicknesses, the thickness error between the expected printing from the manufacturer and the experimental measurement was 0.15 ± 0.02 mm. Table 4 shows the biomechanical properties of the Filastic™ material with different thicknesses.

Table 2. Thickness, failure stress, and maximum Young's modulus values in both longitudinal and circumferential directions

Location	Thickness (mm)	Failure stress (MPa)		Maximum Young's modulus (MPa)	
		L	C	L	C
Medial proximal	1.66	0.46	0.45	0.75	0.89
Medial middle	1.72	0.47	0.61	0.72	1.05
	1.80	0.46	0.64	0.61	0.98
Medial distal	1.63	0.31	0.36	0.61	0.74
Lateral middle	1.06	0.48	0.55	1.02	1.34
Lateral distal	1.05	0.48	0.56	1.02	1.19

Abbreviations: C, circumferential; L, longitudinal.

Table 3. Biomechanical properties of the NinjaFlex material according to thickness

Expected thickness (mm)	Measured thickness (mm)	Failure stress (MPa)	Maximum Young's modulus (MPa)
0.8	0.78	1.38	11.90
0.9	0.89	1.33	8.53
1	0.97	1.38	9.75
1.1	1.05	1.13	8.18
1.2	1.11	0.93	8.88
1.3	1.23	1.54	9.87
1.4	1.33	2.49	9.45
1.5	1.40	2.71	10.93
1.6	1.49	2.80	11.24
1.7	1.53	2.83	10.51
1.8	1.67	2.95	10.26

Table 4. Biomechanical properties of the Filastic™ material according to thickness

Expected thickness (mm)	Measured thickness (mm)	Failure stress (MPa)	Maximum Young's modulus (MPa)
0.5	0.32	2.39	12.65
0.55	0.37	2.37	13.97
0.6	0.45	2.11	21.06
0.65	0.50	2.64	23.16
0.7	0.57	2.38	18.26
0.75	0.62	2.30	12.63
0.8	0.64	2.61	25.37
0.85	0.71	2.53	8.91

Its failure stress and maximum Young's modulus did not increase with thickness. It displayed a highly heterogeneous behavior. With a thickness of 0.65 mm, its failure stress and maximum Young's modulus attained the highest value with 2.64 MPa and 23.16 MPa, respectively.

3.1.3. Rubber-like material (RGD450+TangoPlus)

Ten samples of RGD450+TangoPlus were tested with the biaxial tensile technique. The expected printed thickness values provided by the manufacturer of RGD450+TangoPlus material in the 70 SH and 60 SH were

similar (within 0.03 mm) to the ones measured during the experiment. However, the 50 SH and 40 SH materials showed errors up to 0.45 mm. Table 5 displays the thickness, failure stress, and maximum Young's modulus in both directions (A and B).

As RGD450+TangoPlus was printed for different values of stiffness, we showed that the 70 SH was the stiffest, whereas the 40 SH was the least stiff. Theoretically, materials with the same shore hardness should have the same maximum Young's modulus value regardless of

Table 5. Biomechanical properties of the RGD450+TangoPlus material according to different thicknesses and SH

Shore degree	Expected thickness (mm)	Measured thickness (mm)	Failure stress (MPa)		Maximum elastic modulus (MPa)	
			Direction A	Direction B	Direction A	Direction B
70 SH	2	1.97	0.92	0.82	3.71	3.82
60 SH	2	1.98	0.48	0.57	2.91	2.64
50 SH	2	2.37	0.31	0.26	1.04	1.06
	2.5	2.81	0.22	0.20	1.25	1.11
	3	3.37	0.21	0.16	1.13	1.09
	3.5	3.91	0.22	0.22	1.06	1.06
40 SH	2.5	2.78	0.18	0.15	1.05	0.99
	3	3.44	0.16	0.14	0.82	0.95
	3.5	4.19	0.17	0.17	0.75	0.70
	4	4.49	0.20	0.18	0.74	0.76

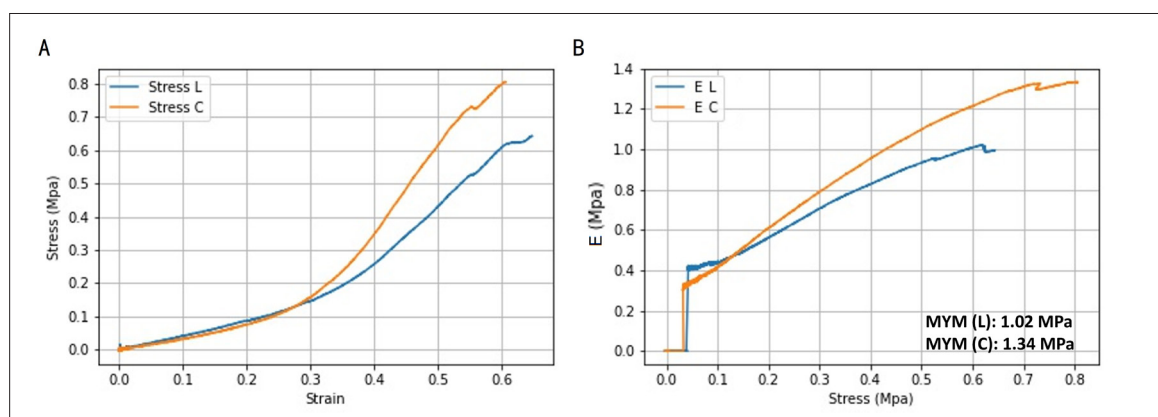


Figure 4. Graphs of biomechanical properties of the healthy aortic wall. (A) Strain–stress curve of the healthy aorta. (B) Stress–Young’s modulus curve of the healthy aorta. Abbreviations: C, circumferential; E, Young’s modulus; L, longitudinal; MYM, maximum Young’s modulus.

the thickness. However, there was no difference in the maximum Young’s modulus between directions A and B ($p > 0.05$) given a variation of stiffness in the 40 SH and 50 SH from 0.70 to 1.05 MPa and 1.04 to 1.25 MPa, respectively.

3.2. Stress–strain curve

The stress–strain and stress–Young’s modulus curves located in the lateral middle aorta were computed (Figure 4).

For the NinjaFlex material, the stress–strain and stress–Young’s modulus curves, which can represent its biomechanical properties, are shown in Figure 5.

Compared with the healthy aortic wall, a higher nonlinearity trend was observed in the printed NinjaFlex material.

The Filastic™ material with different thicknesses was also tested. According to Table 4, the least stiff sample, which showed a biomechanical behavior close to that of the healthy human aorta, was the one with a thickness

of 0.5 mm. Figure 5 shows graphs of the biomechanical properties of this specimen.

Higher stiffness (maximum Young’s modulus) was observed in the NinjaFlex material than in the Filastic™ material. Furthermore, from a biomechanical point of view, both of them showed higher stiffness compared to the healthy human aorta.

According to Table 5, the 2-mm-thick 50-SH RGD450+TangoPlus material had a similar maximum Young’s modulus value as the healthy human aorta. However, it had a lower failure stress value than the healthy aorta (Figure 7).

4. Discussion

According to Sherifova and Holzapfel, large variations can be observed in tissue strength and failure stress^[11] with different test machines and experimental setups. In order to maintain the consistency of the experiments in this study, the experiments were performed using the same machine with the same experimental setup. To our knowledge,

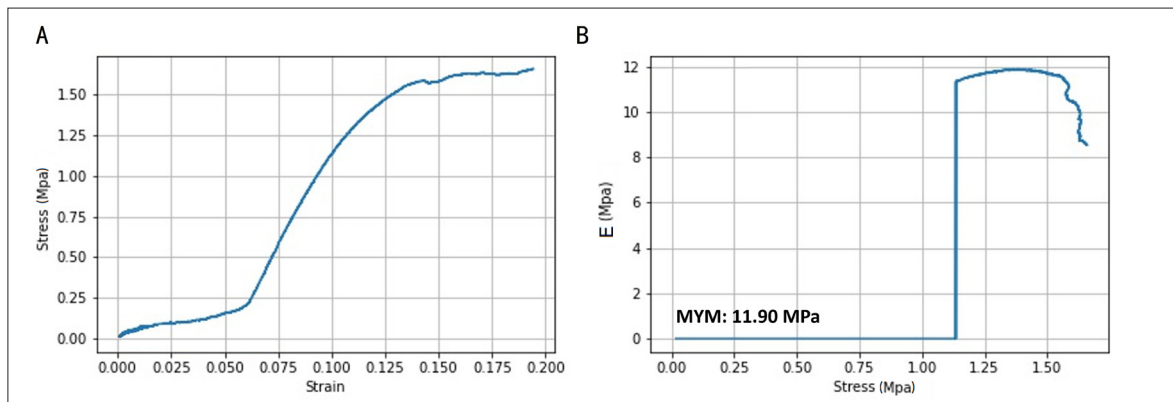


Figure 5. Graphs of biomechanical properties of the NinjaFlex specimen (0.8 mm in thickness). (A) Strain–stress curve. (B) Stress–Young’s modulus curve. Abbreviations: E, Young’s modulus; MYM, maximum Young’s modulus.

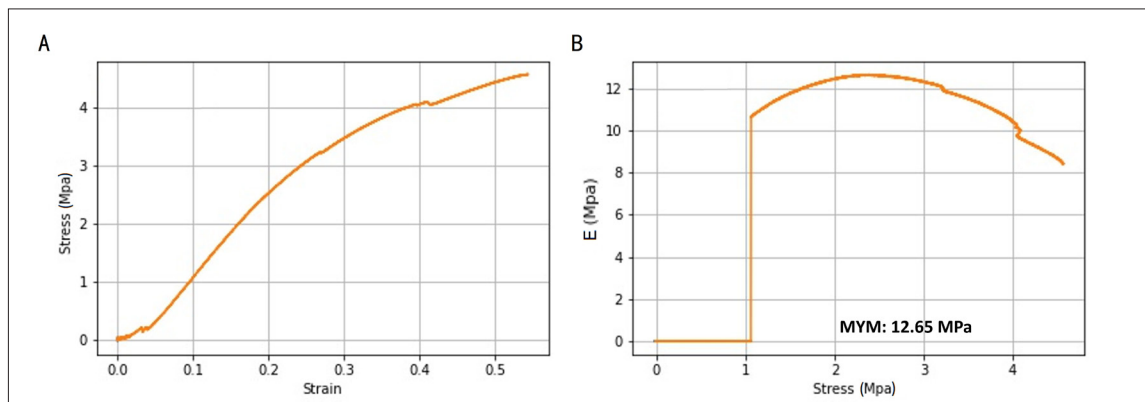


Figure 6. Graphs of biomechanical properties of Filastic™ (0.5 mm). (A) Strain–stress curve. (B) Stress–Young’s modulus curve. Abbreviations: E, Young’s modulus; MYM, maximum Young’s modulus.

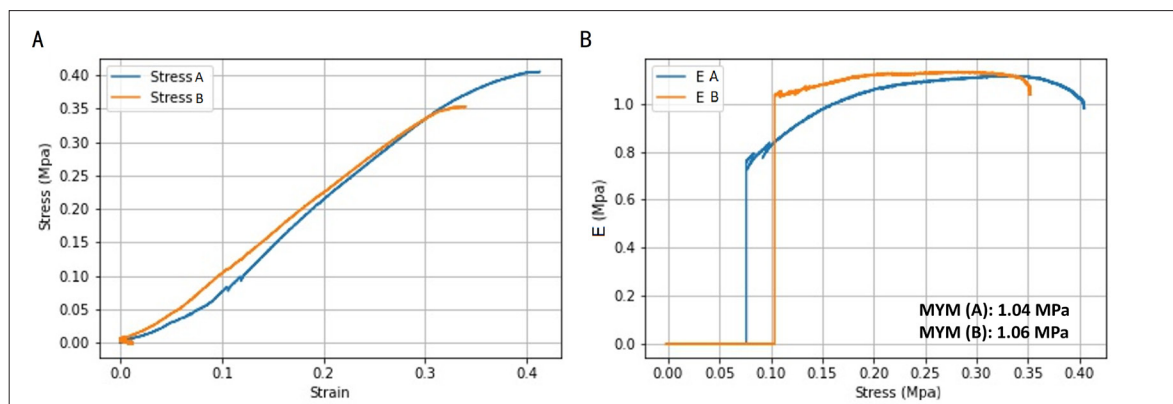


Figure 7. Graphs of biomechanical properties of RGD450+TangoPlus (2 mm, 50 SH). (A) Strain–stress curve. (B) Stress–Young’s modulus curve. Abbreviations: E, Young’s modulus; MYM, maximum Young’s modulus.

there is no existing reference of a 3D-printed human aorta with acceptable biomechanical properties. Thermoplastic polyurethane and rubber-like materials are commonly used in 3D-printed artery studies^[26]. The aim of our study was to obtain a common synthetic material for *in vitro* study. Hence, three different nonbiocompatible materials

(NinjaFlex, Filastic™, and RGD450+TangoPlus) were tested to identify a material that has similar biomechanical properties to that of a healthy human aorta. If we are aware of the biomechanical properties of the proposed material (such as its maximum Young’s modulus value), and if these properties resemble the behavior of the aorta, data-

acquired CFD modeling on phantoms designed with this material would be reinforced and more credible for clinical comparisons. Concerning the design of the samples, a noticeable difference was found between the expected thickness and the one measured experimentally. Among the three materials, the Filastic™ material had the smallest thickness error (maximum difference of 10.12%), while the NinjaFlex had the largest error (maximum difference of 33.09%). The thickness error in RGD450+TangoPlus samples ranged from 0.85% to 19.57%. According to Chung *et al.*, a slower printing speed can reduce thickness error, thus achieving higher model accuracy (between computer-aided design [CAD] models and physical models)^[26]. Our study showed that thickness error was greater in thicker samples and differed between printing materials.

The aortic wall is normally considered anisotropic and nonlinear^[11,27-32]. All of the three printed materials showed a nonlinear behavior. However, since the 3D-printed material is synthetic, it is difficult to mimic the anisotropic behavior. Although RGD450+TangoPlus showed small differences in the value of maximum Young's modulus in directions A and B, the difference between the two directions was not statistically significant.

In other similar studies on the biomechanical properties of the human aorta, the range of failure stress was found to be between 0.54 MPa and 2.18 MPa^[30,33-37]. In our study of the healthy aorta, the mean failure stress value was 0.48 MPa, with a maximum Young's modulus of 0.91 MPa. Compared with thermoplastic polyurethane, RGD450+TangoPlus had by far the closest biomechanical properties to the healthy aortic wall (0.28 MPa in stress and 1.05 MPa in maximum Young's modulus).

5. Conclusion

RGD450+TangoPlus in 50 SH is the most suitable 3D printable material (among the three synthetic materials tested in this study) to represent a healthy human aorta although thermoplastic polyurethane has a lower cost and easier setup compared to rubber-like material^[26].

Acknowledgments

We thank the association of "Bourgogne Coeur" and EU funds PO FEDER-FSE Bourgogne 2012-2020 for the financial support in the experiments. We also thank Dijon 3D company (Dijon, France) for providing the thermoplastic polyurethane material.

Funding

This study was financed by the association of "Bourgogne Coeur" and the EU funds PO FEDER-FSE Bourgogne 2012-2020.

Conflict of interest

The authors declare no conflict of interests.

Author contributions

Conceptualization: Siyu Lin, Olivier Bouchot

Data curation: Siyu Lin

Formal analysis: Siyu Lin

Funding acquisition: Olivier Bouchot

Investigation: Siyu Lin, Chloe Bernard, Moundji Kafi

Methodology: Siyu Lin

Project administration: Alain Lalande, Olivier Bouchot

Resources: Georges Tarris, Chloe Bernard, Camille Gobled

Software: Siyu Lin, Diana M. Marín-Castrillón, Arnaud Boucher, Benoit Presles

Supervision: Alain Lalande, Olivier Bouchot

Validation: Siyu Lin

Visualization: Siyu Lin, Alain Lalande, Paul M. Walker

Writing – original draft: Siyu Lin

Writing – review & editing: Alain Lalande, Paul M. Walker, Olivier Bouchot

Investigation: Siyu Lin, Chloe Bernard, Moundji Kafi, Marie-Catherine Morgant

Consent for publication

With regard to Jardé law (French Bioethics law), patient consent was waived as autopsy samples are not concerned by bioethical regulations.

Availability of data

The datasets generated during and/or analyzed during the current study are available from the corresponding author on reasonable request.

References

1. Ploch CC, Mansi CSSA, Jayamohan J, *et al.*, 2016, Using 3D printing to create personalized brain models for neurosurgical training and preoperative planning. *World Neurosurg*, 90:668–674.
<https://doi.org/10.1016/j.wneu.2016.02.081>
2. Hochman JB, Rhodes C, Wong D, *et al.*, 2015, Comparison of cadaveric and isomorphic three-dimensional printed models in temporal bone education. *Laryngoscope*, 125(10):2353–2357.
<https://doi.org/10.1002/lary.24919>
3. Lynn AQ, Pflibsen LR, Smith AA, *et al.*, 2021, Three-dimensional printing in plastic surgery: Current applications, future directions, and ethical implications. *Plast Reconstr Surg Glob Open*, 9(3):e3465.
<https://doi.org/10.1097/GOX.0000000000003465>

4. Lal H., Patralekh MK, 2018, 3D printing and its applications in orthopaedic trauma: A technological marvel. *J Clin Orthop Trauma*, 9(3):260–268.
<https://doi.org/10.1016/j.jcot.2018.07.022>
5. Khorsandi D, Fahimipour A, Abasian P, *et al.*, 2021, 3D and 4D printing in dentistry and maxillofacial surgery: Printing techniques, materials, and applications. *Acta Biomater*, 122:26–49.
<https://doi.org/10.1016/j.actbio.2020.12.044>
6. Wang Z, Wang L, Li T, *et al.*, 2021, 3D bioprinting in cardiac tissue engineering. *Theranostics*, 11(16):7948–7969.
<https://doi.org/10.7150/thno.61621>
7. Brantner P, Madaffari A, Fahrni G, *et al.*, 2020, 3D-printed visualization of a complex coronary-venous fistula with additional feeders from the descending aorta. *JACC Case Rep*, 2(11):1736–1738.
<https://doi.org/10.1016/j.jaccas.2020.06.028>
8. Santoro G, Pizzuto A, Rizza A, *et al.*, 2021, Transcatheter treatment of ‘complex’ aortic coarctation guided by printed 3D model. *JACC Case Rep*, 3(6):900–904.
<https://doi.org/10.1016/j.jaccas.2021.04.036>
9. Kim WK, Kim T, Lee S, *et al.*, 2019, 3D-printing-based open repair of extensive thoracoabdominal aorta in severe scoliosis. *Semin Thorac Cardiovasc Surg*, 31(1):61–63.
<https://doi.org/10.1053/j.semtcvs.2018.09.017>
10. Ooms JF, Wang DD, Rajani R, *et al.*, 2021, Computed tomography-derived 3D modeling to guide sizing and planning of transcatheter mitral valve interventions. *JACC Cardiovasc Imaging*, 14(8): 1644–1658.
<https://doi.org/10.1016/j.jcmg.2020.12.034>
11. Sherifova S, Holzapfel GA, 2019, Biomechanics of aortic wall failure with a focus on dissection and aneurysm: A review. *Acta Biomater*, 99:1–17.
<https://doi.org/10.1016/j.actbio.2019.08.017>
12. Lin S, Morgant MC, Marín-Castrillón DM, *et al.*, 2022, Aortic local biomechanical properties in ascending aortic aneurysms. *Acta Biomater*, 149:40–50 .
<https://doi.org/10.1016/j.actbio.2022.06.019>
13. Community challenge towards consensus on characterization of biological tissue. *C4Bio*.
<https://c4bio.eu/> (accessed Dec. 10, 2022).
14. Caballero AD, Laín S, 2013, A review on computational fluid dynamics modelling in human thoracic aorta. *Cardiovasc Eng Technol*, 4(2):103–130.
<https://doi.org/10.1007/s13239-013-0146-6>
15. Ong CW, Wee I, Syn N, *et al.*, 2020, Computational fluid dynamics modeling of hemodynamic parameters in the human diseased aorta: A systematic review. *Ann Vasc Surg*, 63:336–381.
<https://doi.org/10.1016/j.avsg.2019.04.032>
16. Mourato A, Valente R, Xavier J, *et al.*, 2022, Computational modelling and simulation of fluid structure interaction in aortic aneurysms: A systematic review and discussion of the clinical potential. *Appl Sci*, 12(16):8049.
<https://doi.org/10.3390/app12168049>
17. Vignali E, Gasparotti E, Celi S, *et al.*, 2021, Fully-coupled FSI computational analyses in the ascending thoracic aorta using patient-specific conditions and anisotropic material properties. *Front Physiol*, 12:732561.
<https://doi.org/10.3389/fphys.2021.732561>
18. Simão M, Ferreira J, Tomás AC, *et al.*, 2017, Aorta ascending aneurysm analysis using CFD models towards possible anomalies. *Fluids*, 2(2):31.
<https://doi.org/10.3390/fluids2020031>
19. Wee I, Ong CW, Syn N, *et al.*, 2018, Computational fluid dynamics and aortic dissections: Panacea or panic? *Vasc Endovasc Rev*, 1(1):27–29.
<https://doi.org/10.15420/ver.2018.8.2>
20. Wang Y, Joannic D, Juillion P, *et al.*, 2016, Comparison of flow measurement by 4D flow magnetic resonance imaging and by particles image velocimetry on phantom of abdominal aortic aneurysm. *SM Vasc Med*, 1(2):1008.
<https://hal.archives-ouvertes.fr/hal-01463873>
21. Kurenov SN, Ionita C, Sammons D, *et al.*, 2015, Three-dimensional printing to facilitate anatomic study, device development, simulation, and planning in thoracic surgery. *J Thorac Cardiovasc Surg*, 149(4):973–979.
<https://doi.org/10.1016/j.jtcvs.2014.12.059>
22. Vukicevic M, Puperi DS, Grande-Allen KJ, *et al.*, 2016, Erratum to: 3D printed modeling of the mitral valve for catheter-based structural interventions. *Ann Biomed Eng*, 44(11):3432–3432.
<https://doi.org/10.1007/s10439-016-1690-7>
23. Wang K, Wu C, Qian Z, *et al.*, 2016, Dual-material 3D printed metamaterials with tunable mechanical properties for patient-specific tissue-mimicking phantoms. *Addit Manuf*, 12:31–37.
<https://doi.org/10.1016/j.addma.2016.06.006>
24. Biglino G, Verschueren P, Zegels R, *et al.*, 2013, Rapid prototyping compliant arterial phantoms for in-vitro studies and device testing. *J Cardiovasc Magn Reson*, 15(1):2.
<https://doi.org/10.1186/1532-429X-15-2>
25. Duprey A, Khanafer K, Schlicht M, *et al.*, 2010, In vitro characterisation of physiological and maximum elastic

- modulus of ascending thoracic aortic aneurysms using uniaxial tensile testing. *Eur J Vasc Endovasc Surg*, 39(6):700–707.
<https://doi.org/10.1016/j.ejvs.2010.02.015>
26. Chung M, Radacsi N, Robert C, *et al.*, 2018, On the optimization of low-cost FDM 3D printers for accurate replication of patient-specific abdominal aortic aneurysm geometry. *3D Print Med*, 4(1):2.
<https://doi.org/10.1186/s41205-017-0023-2>
 27. Iliopoulos DC, Deveja RP, Kritharis EP, *et al.*, 2009, Regional and directional variations in the mechanical properties of ascending thoracic aortic aneurysms. *Med Eng Phys*, 31(1):1–9.
<https://doi.org/10.1016/j.medengphy.2008.03.002>
 28. Ferrara A, Morganti S, Totaro P, *et al.*, 2016, Human dilated ascending aorta: Mechanical characterization via uniaxial tensile tests. *J Mech Behav Biomed Mater*, 53:257–271.
<https://doi.org/10.1016/j.jmbbm.2015.08.021>
 29. Ferrara A, Totaro P, Morganti S, *et al.*, 2018, Effects of clinico-pathological risk factors on in-vitro mechanical properties of human dilated ascending aorta. *J Mech Behav Biomed Mater*, 77:1–11.
<https://doi.org/10.1016/j.jmbbm.2017.08.032>
 30. Vande Geest JP, Sacks MS, Vorp DA, 2006, The effects of aneurysm on the biaxial mechanical behavior of human abdominal aorta. *J Biomech*, 39(7):1324–1334.
<https://doi.org/10.1016/j.jbiomech.2005.03.003>
 31. Azadani AN, Chitsaz S, Mannion A, *et al.*, 2013, Biomechanical properties of human ascending thoracic aortic aneurysms. *Ann Thorac Surg*, 96(1):50–58.
<https://doi.org/10.1016/j.athoracsur.2013.03.094>
 32. Pham T, Martin C, Elefteriades J, *et al.*, 2013, Biomechanical characterization of ascending aortic aneurysm with concomitant bicuspid aortic valve and bovine aortic arch. *Acta Biomater*, 9(8):7927–7936.
<https://doi.org/10.1016/j.actbio.2013.04.021>
 33. Raghavan ML, Webster MW, Vorp DA, 1996, Ex vivo biomechanical behavior of abdominal aortic aneurysm: Assessment using a new mathematical model. *Ann Biomed Eng*, 24(5):573–582.
<https://doi.org/10.1007/BF02684226>
 34. Vorp DA, Schiro BJ, Ehrlich MP, *et al.*, 2003, Effect of aneurysm on the tensile strength and biomechanical behavior of the ascending thoracic aorta. *Ann Thorac Surg*, 75(4):1210–1214.
[https://doi.org/10.1016/S0003-4975\(02\)04711-2](https://doi.org/10.1016/S0003-4975(02)04711-2)
 35. Di Martino ES, Bohra A, Vande Geest JP, *et al.*, 2006, Biomechanical properties of ruptured versus electively repaired abdominal aortic aneurysm wall tissue. *J Vasc Surg*, 43(3):570–576.
<https://doi.org/10.1016/j.jvs.2005.10.072>
 36. Sommer G, Sherifova S, Oberwalder PJ, *et al.*, 2016, Mechanical strength of aneurysmatic and dissected human thoracic aortas at different shear loading modes. *J Biomech*, 49(12):2374–2382.
<https://doi.org/10.1016/j.jbiomech.2016.02.042>
 37. García-Herrera CM, Atienza JM, Rojo FJ, *et al.*, 2012, Mechanical behaviour and rupture of normal and pathological human ascending aortic wall. *Med Biol Eng Comput*, 50(6):559–566.
<https://doi.org/10.1007/s11517-012-0876-x>